Astron. Astrophys. 309, 612–628 (1996)

ASTRONOMY AND ASTROPHYSICS

Mid-infrared spectroscopy of carbon-rich post-AGB objects and detection of the PAH molecule chrysene

K. Justtanont[1,2,3], M.J. Barlow[2], C.J. Skinner[4], P.F. Roche[5], D.K Aitken[6], and C.H. Smith[6]

[1] NASA Ames Research Center, MS 245-3, Moffett Field, CA 94035, USA
[2] Department of Physics and Astronomy, University College London, Gower Street, London, WC1E 6BT, UK
[3] Institut d'Astrophysique de Paris, 98 bis Bld. Arago, F-75014 Paris, France
[4] Institute of Geophysics and Planetary Physics, Lawrence Livermore National Laboratory, PO Box 808, CA 94581-9900, USA
[5] Astrophysics, Physics Department, Oxford University, Keble Road, Oxford OX1 3RH, UK
[6] Department of Physics, University College, ADFA, Campbell, ACT 2600, Australia

Received 17 January 1995 / Accepted 18 September 1995

Abstract. We present 10 and 20-μm spectroscopic observations of a sample of F- and G-type carbon-rich post-AGB objects, three of which were known to exhibit the unidentified emission feature at 21 μm. We also find the F3I post-AGB object SAO 163075 to exhibit a (weak) 21-μm emission feature. We additionally obtained a 10-μm spectrum of IRAS 05341+0852, which has been reported to have a possible 21-μm emission band in its *IRAS* LRS spectrum, and obtained new 10 and 20-μm spectra of the carbon-rich bipolar post-AGB sources GL 2688 and GL 618, the extreme carbon star GL 3068, and the planetary nebulae IRAS 21282+5050 and He 2-447, in order to study the evolution of C-rich dust from the early post-AGB through to the planetary nebula (PN) phases. The 7.5–13-μm spectra of the 21-μm band objects exhibit broad plateau emission, shortwards of 9 μm and from 10–13 μm, superposed upon which, in addition to the well-known UIR-band at 11.3 μm, are several new features, at 7.9, 8.2, 10.6, 11.5 and 12.2 μm, differing from those observed in standard UIR-band spectra. An excellent match is found between the wavelengths of these new features and those of bands in the spectrum of chrysene ($C_{18}H_{12}$), one of the simplest PAH molecules. The absence of the new features in the spectra of earlier spectral-type post-AGB objects and PN is consistent with the expected complete dehydrogenation of any PAH molecules having less than 20-25 carbon atoms when exposed to the ultraviolet radiation fields of stars with spectral types earlier than F. Chrysene is not responsible for the 21-μm emission bands observed in the spectra of the cool post-AGB objects. Possible identifications for the 21-μm band in terms of highly hydrogenated 2-dimensional PAH molecules or 3-dimensional fulleranes (hydrogenated fullerenes) are discussed. The mid-infrared spectrum of GL 2688 is largely featureless, apart from two broad weak emission features between 9.5–10.5 and 10.5–12.2 μm. The profiles of the broad 10–13-μm absorption features in the spectra of the extreme carbon star GL 3068 and the C-rich bipolar post-AGB object GL 618 are compared. For GL 3068 the profile shape and the wavelength of peak absorption, near 11 μm, are consistent with absorption by silicon carbide particles. However, the absorption observed towards GL 618 is considerably broader and peaks at 12 μm. Its profile is very similar to that of the 10–13-μm emission plateau observed in the spectra of the 21-μm band objects, suggesting that it arises from absorption by a large column of highly-hydrogenated PAH-type species.

Key words: stars: post-AGB – circumstellar matter – dust – molecular data

1. Introduction

It is generally believed that many Asymptotic Giant Branch (AGB) stars are precursors of planetary nebulae (PN). The *AFGL* and *IRAS* missions discovered a significant number of objects which are thought to be transition objects between the AGB and PN phases, i.e. post-AGB objects. As a star enters the post-AGB phase, the mass loss rate is believed to drop sharply, with the remnant shell of gas and dust formed on the AGB coasting away from the central star at its expansion velocity, so that the central star is then revealed. This results in a double-peaked energy distribution, where the optical/near-IR component is dominated by the stellar radiation while the longer wavelength peak in the mid-infrared is due to the detached dust shell (Volk & Kwok 1989). Many of these post-AGB stars are found to exhibit F- or G-type supergiant spectra (Hrivnak, Kwok & Volk 1989; Trams et al. 1991; Hrivnak 1995), their supergiant-like spectra being a consequence of the low surface gravities resulting from their low masses and large radii and luminosities. A number of these stars have been found to show highly depleted photospheric Fe/H ratios (Luck, Bond & Lambert 1990; Waelkens et al. 1991), which

Send offprint requests to: M.J. Barlow

were initially interpreted as evidence of Population II status. However, the sum of the derived (C+N+O)/H abundances are near-solar and more recently the observed heavy-metal abundance patterns have been interpreted as due to differential depletion onto dust grains (Bond 1991; Mathis & Lamers 1992; Waters, Waelkens & Trams 1992). AGB stars can have either O-rich or C-rich envelopes and can be classified by their dust properties. The main signatures for O-rich post-AGB stars are silicate features and possibly OH masers (Likkel et al. 1991). C-rich post-AGB stars may display the signatures of carbon-rich dust in the form of 10-12 μm silicon carbide emission or the unidentified infrared (UIR) bands with distinct features at 3.3, 6.2, 7.7, 11.3 and 12.7 μm which are usually attributed to polycyclic aromatic hydrocarbons (PAH, Leger & Puget 1984; Allamandola, Tielens & Barker 1985, 1989: hereafter ATB85, ATB89; Leger, d'Hendecourt & Défourneau 1989). At least some of the carriers of these features survive the harsh ultraviolet radiation of the central star as the source evolves to become a planetary nebula (Gillett et al. 1973; Aitken et al. 1979).

Kwok, Volk & Hrivnak (1989) reported a group of four of these evolved objects which exhibited a very strong broad emission feature peaking near 21-μm. Their infrared energy distributions show the usual characteristic double-peak associated with detached dust shells. Hrivnak & Kwok (1991) added another source to this group, while Kwok et al. (1993) added a further four sources showing 21-μm band emission. All of the 21-μm band sources so far studied in detail in the optical have been found to have C-rich photospheres (e.g. Hrivnak & Kwok 1991; Hrivnak 1995), while Omont et al. (1993) inferred carbon-rich environments from their large observed HCN/CO millimetre-line intensity ratios. This, together with the detection of various PAH-like features in their infrared spectra, strongly suggests that the 21-μm band carriers are carbon-based (Kwok et al. 1989; Buss et al. 1990, 1993). Geballe et al. (1992) found unusually strong 3.4 and 3.5 μm features, relative to the usually-dominant 3.3 μm feature, in the spectra of two of the 21-μm band objects (IRAS 04296+3429 and IRAS 22272+5435), as well as that of GL 2688, emphasising the unusual nature of the spectra of these objects throughout the near- and mid-infrared.

In order to study the dust properties of these objects in more detail, we have obtained mid-infrared spectra of three objects with 21-μm emission bands from the list of Kwok et al. (1989), IRAS 04296+3429, 07134+1005 and 22272+5435, and of one 21-μm band source from the list of Kwok et al. (1993), IRAS 05341+0852, which Geballe and van der Veen (1990) found to have a 3.4 μm emission band which, uniquely, is stronger than its 3.3 μm emission band. In addition, we also include here mid-infrared spectra of SAO 163075, since our data indicate that it may possess a rather weak 21-μm emission band. As these objects are expected to have evolved from AGB stars, and to evolve into PNe, we also present spectra of the extreme carbon star GL 3068, the well-studied post-AGB objects GL 618, and GL 2688, and the PNe He 2–447 and IRAS 21282+5050, as comparisons. The observations of these sources are described in Sect. 2 and the spectral features detected are discussed in Sect. 3.

2. Observations

Spectra at 8–13 μm of IRAS 04296+3429, 05341+0852 and 22272+5435 (= SAO 34504), GL 2688 and of He 2–447 were obtained with the UCL Spectrometer on the 3.8 m UKIRT in 1990. An aperture of 4.5 arcsec diameter was employed with standard chopping and beam-switching techniques. The spectral resolutions were $\Delta\lambda = 0.09$ μm for IRAS 05341+0852 and 22272+5435, and $\Delta\lambda = 0.24$ μm for IRAS 04296+3429 and He 2-447.

Between 1990 and 1993 we used the common-user Cooled Grating Spectrometer 3 (CGS3) on UKIRT to obtain 10 and 20 μm spectra of IRAS 04296+3429, 07134+1005 (= SAO 96709) and 22272+5435, as well as of SAO 163075, GL 2688, GL 618, GL 3068 and IRAS 21282+5050. The spectrometer contains an array of 32 discrete As:Si photoconductive detectors, and three interchangeable permanently mounted gratings covering the 10 μm and 20 μm atmospheric windows. Two grating settings give a fully sampled 64-point spectrum of the chosen waveband. The 10 μm low resolution grating covers the wavelength range 7.4–13.3 μm with a resolution of 0.18 μm, while the 20 μm grating covers the range 15.4–24.1 μm with a resolution of 0.27 μm; the atmosphere is opaque between 13.5 and 16 μm. In addition, we obtained further spectra of IRAS 04296+3429 using a higher resolution CGS3 10 μm grating ($\Delta\lambda = 0.05$ μm), centering the spectra at 10.7 μm and 12.1 μm to obtain continuous coverage from 9.95–13.1 μm. All spectra were taken through a 5.5 arcsec aperture, except for GL 2688, where we employed a 9 arcsec aperture because the nebula was found to be extended at 10 μm.

The spectra were flux-calibrated with respect to β And, α Tau, α Boo and β Peg. Residual structure arising from incomplete cancellation of the strong telluric ozone absorption band at 9.7 μm is present in some of the spectra after dividing by the standard star. Details of the observations are listed in Table 1. In order to show the full detail present in the 10 μm spectra, each 10 μm spectrum is shown separately in Fig. 1, while Fig. 2 shows the 10 *and* 20 μm spectra of each object. Note that Figs. 1(a) and (b) show the UCLS 10 μm spectra of IRAS 22272+5435 and 04296+3429, while Figs. 2(a) and (b) show the CGS3 10 and 20 μm spectra of these objects.

Since many post-AGB stars are known to vary in the optical (Fernie 1983; Hrivnak, Kwok & Geballe 1994), we have not adjusted the flux levels of the 10 and 20 μm spectra shown in Figs. 1 and 2 to make them agree with either the *IRAS* broad-band 12 and 25μm fluxes or with the *IRAS* LRS fluxes. We note that the flux levels of the CGS3 10 μm spectrum of IRAS 04296+3429 in Fig. 2b is only 65 percent of that in the UCLS spectrum plotted in Fig. 1(b), and that there is a smaller discrepancy between the flux levels in the UCLS and CGS3 spectra of IRAS 22272+5435 in Figs. 1(a) and 2(a). We are reluctant to ascribe these differences to real variability in the mid-infrared fluxes and believe that they caused by differences in the apertures, seeing and guiding, etc. In an attempt to separate the emission-band features from an assumed underlying continuum, we subsequently adjusted the flux levels of the individual 10 and 20 μm spectra

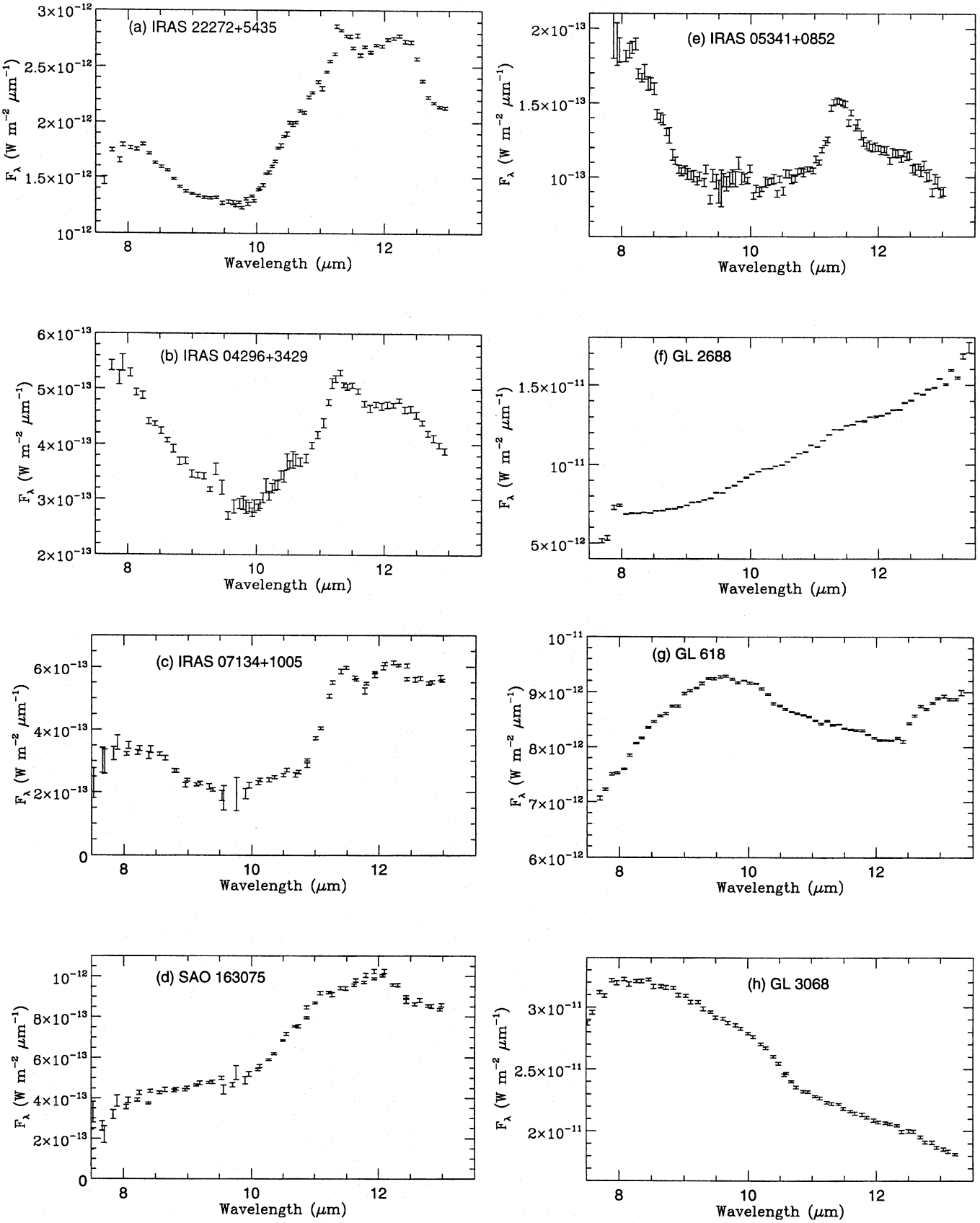

Fig. 1a–j. The 10 μm spectra of the post-AGB and related objects. The sources are ordered as a function of decreasing spectral type for the post-AGB objects (**a**–**g**). **a** IRAS 22272+5435; **b** IRAS 04296+3429; **c** IRAS 07134+1005; **d** SAO 163075; **e** IRAS 05341+0852; **f** GL 2688; **g** GL 618; **h** GL 3068; **i** IRAS 21282+5050; **j** He 2–447

to match those of the *IRAS* LRS spectra and arbitarily defined the continuum level of each 21-μm band object to be given by a black-body which fits the 10.0 and 18.0 μm fluxes. The temperatures corresponding to these blackbody fits were 208, 220, 160, and 190 K for IRAS 22272+5435, 04296+3429, 07134+1005 and SAO 163075, respectively. On subtracting these blackbody curves from the spectra of the 21-μm band objects, the 'excess' band emission can be seen more clearly, particularly in the case of SAO 163075. These 'excess' spectra are illustrated in Fig. 3.

3. Results

3.1. Dust emission in carbon-rich objects

The spectral signatures of carbon-rich dust grains have been established through observations of carbon stars and planetary nebulae. The spectra of dusty carbon stars often show a broad emission feature peaking near 11.2 μm and attributed to silicon carbide (Treffers & Cohen 1974; Merrill & Stein 1976a,b). In many cases the SiC feature is accompanied by a featureless emission component with a colour temperature close to 1000 K, which on abundance arguments is attributed to carbon grains, either in the form of graphite or a more amorphous structure. The shape of the SiC emission feature has been investigated by Cohen (1984) who finds evidence for some variations in the emission profile, but the emission appears to be confined to the region between 10.2 and 12.8 μm with a peak in the range 11.0–11.3 μm. From *IRAS* LRS spectra, Little-Marenin (1986) found a SiC peak at 11.15 μm and a FWHM of 1.6 μm. From laboratory measurements (e.g. Friedemann et al. 1981; Borghesi et al. 1985), α- and β-SiC have extinction peaks at 11.4 and 11.1 μm, respectively. A similar emission feature to that in carbon stars is seen in the spectra of many carbon-rich planetary nebulae (Willner et al. 1979; Aitken et al. 1979). However, the SiC band is often accompanied by a series of narrow emission bands between 3 and 13 microns (Aitken & Roche 1982) known as the unidentified infrared (UIR) emission bands and attributed to C-H and C-C transitions in UV-excited, carbon-rich hydrocarbon molecules. More specific identifications of the species that produce the UIR bands have been made with hydrogenated amorphous carbon (HAC, Duley & Williams 1981) and with polycyclic aromatic hydrocarbons (PAH) (Leger & Puget 1984, ATB85). For planetary nebulae, objects with carbon-to-oxygen ratios only slightly greater than unity display the SiC feature strongly, but with increasing C/O ratio the UIR bands increasingly dominate the spectra (Barlow 1983; Cohen et al. 1986, 1989; Roche 1989).

The UIR bands form a fairly well-defined family of emission features with principal members at 3.3, 6.2, 7.7, 8.6 and 11.3 microns which generally appear together with similar band profiles and relative intensities from source to source. There are clear variations in the detailed band profiles in some objects and several weaker emission bands have been detected (between 3.4 and 3.6 μm and at 5.2, 11.1 and 12.7 μm; Russell, Soifer & Willner 1977; de Muizon et al. 1986, ATB89, Roche, Aitken & Smith 1991). Nonetheless, a fairly standard UIR band spectrum is seen

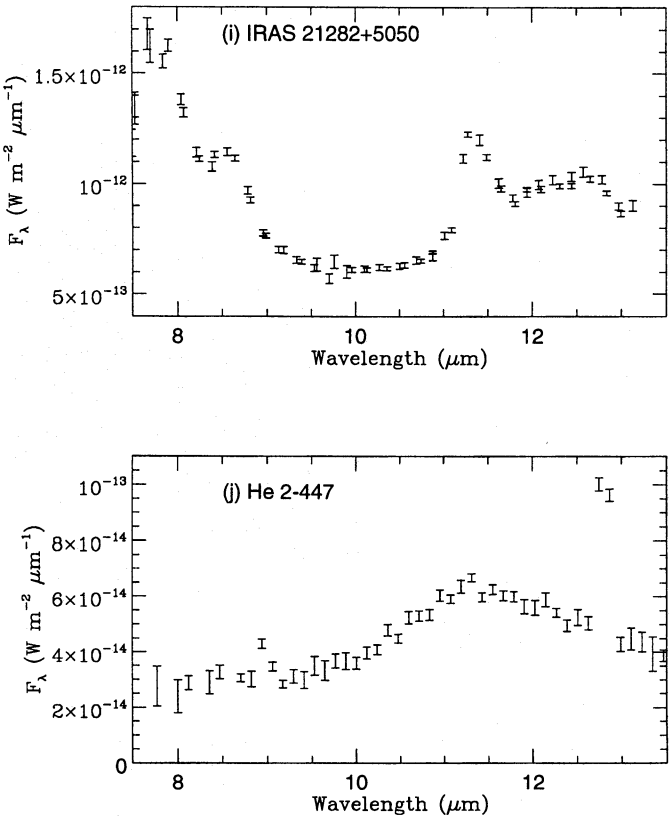

Fig. 1a–j. (continued)

in a variety of sources excited by hot stars, including the nuclei of H II region galaxies, Galactic H II regions, reflection nebulae, planetary nebulae and evolved stars, and in most objects the similarities are much more marked than the differences.

We show in Figs. 1i and 1j the 8–13 μm spectra of two representative planetary nebula which display the standard carbon-rich dust emission signatures in evolved objects. He 2–447 (Fig. 1j) shows a clear broad emission peak at 11.2 μm, which is representative of the SiC emission feature, together with [Ar III] and [Ne II] ionic emission lines at 9.0 and 12.8 μm. IRAS 21282+5050 (Fig. 1i) has very weak ionic line emission, and displays a typical UIR band spectrum with a marked asymmetry in the 11.3 μm feature, a strong emission plateau between 11 and 13 μm, a weak feature at 8.65 μm and the long wavelength wing of the 7.7 μm emission band.

3.2. Emission features in the 10-μm spectra of post-AGB objects

The 10 μm spectra of the optically-visible F- and G-type post-AGB sources displayed in Fig. 1 are complex, with broad emission peaks near 8 μm and 11–12 μm that show some resemblance to the well-known 7.7 μm and 11.3 μm UIR emission bands. The mean central wavelengths of the emission features found in the spectra of three of the 21-μm band objects are listed in Table 2. From the internal agreement between the peak wavelengths measured from different spectra of the same object, we estimate these peak wavelengths to be accurate to $\pm$0.05 μm.

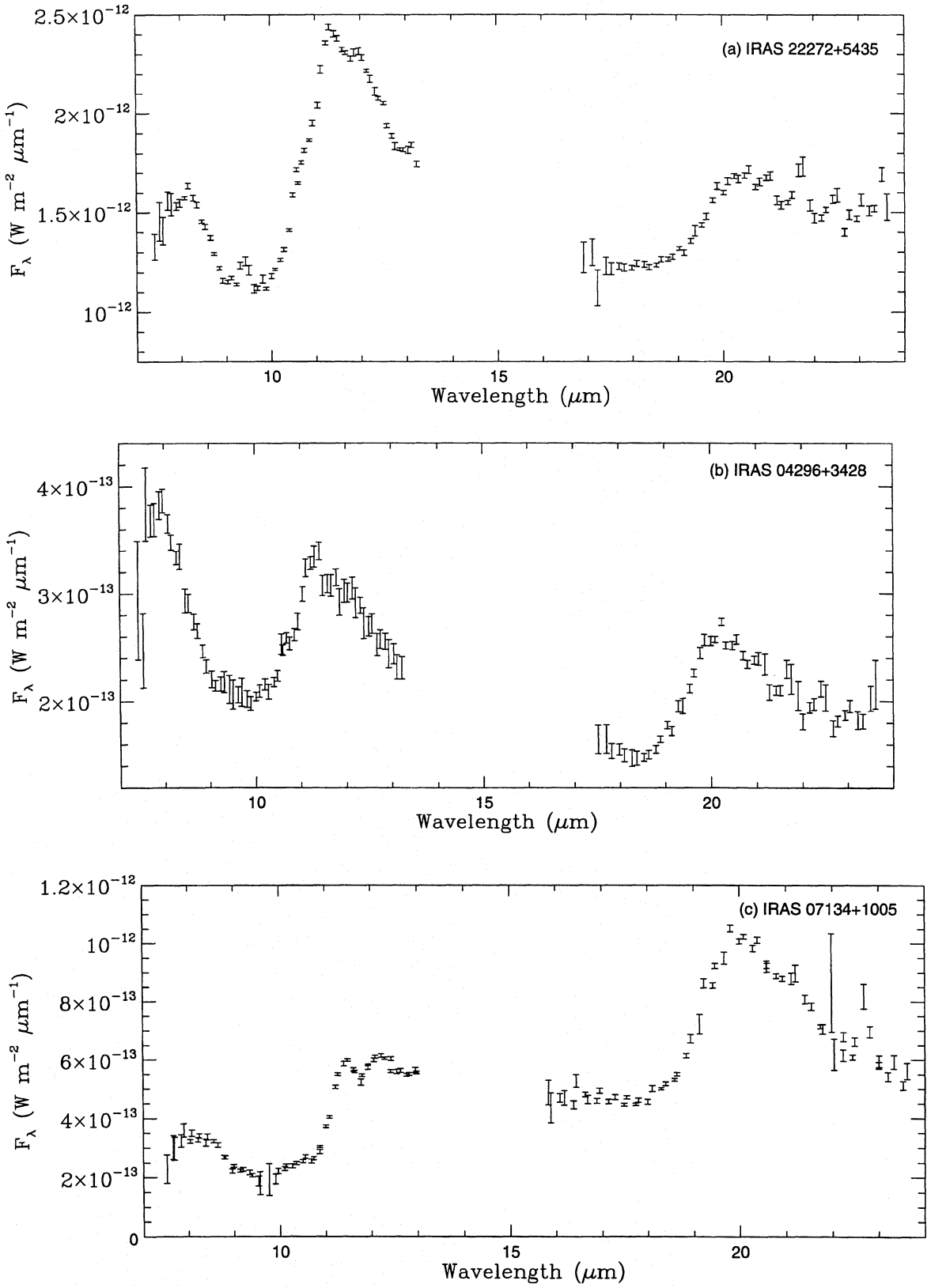

Fig. 2a–h. The 10 and 20 μm spectra of the post-AGB and related objects. The sources are again ordered as a function of decreasing spectral type for the post-AGB objects (**a–f**). **a** IRAS 22272+5435; **b** IRAS 04296+3429; **c** IRAS 07134+1005; **d** SAO 163075; **e** GL 2688; **f** GL 618; **g** GL 3068; **h** IRAS 21282+5050 Note that the 10 and 20-μm spectra illustrated in **a** and **b** for IRAS 22272+5435 and 04296+3429, respectively, were obtained using CGS3, whereas UCLS 10-μm spectra of these objects are shown in Figs. 1a and b

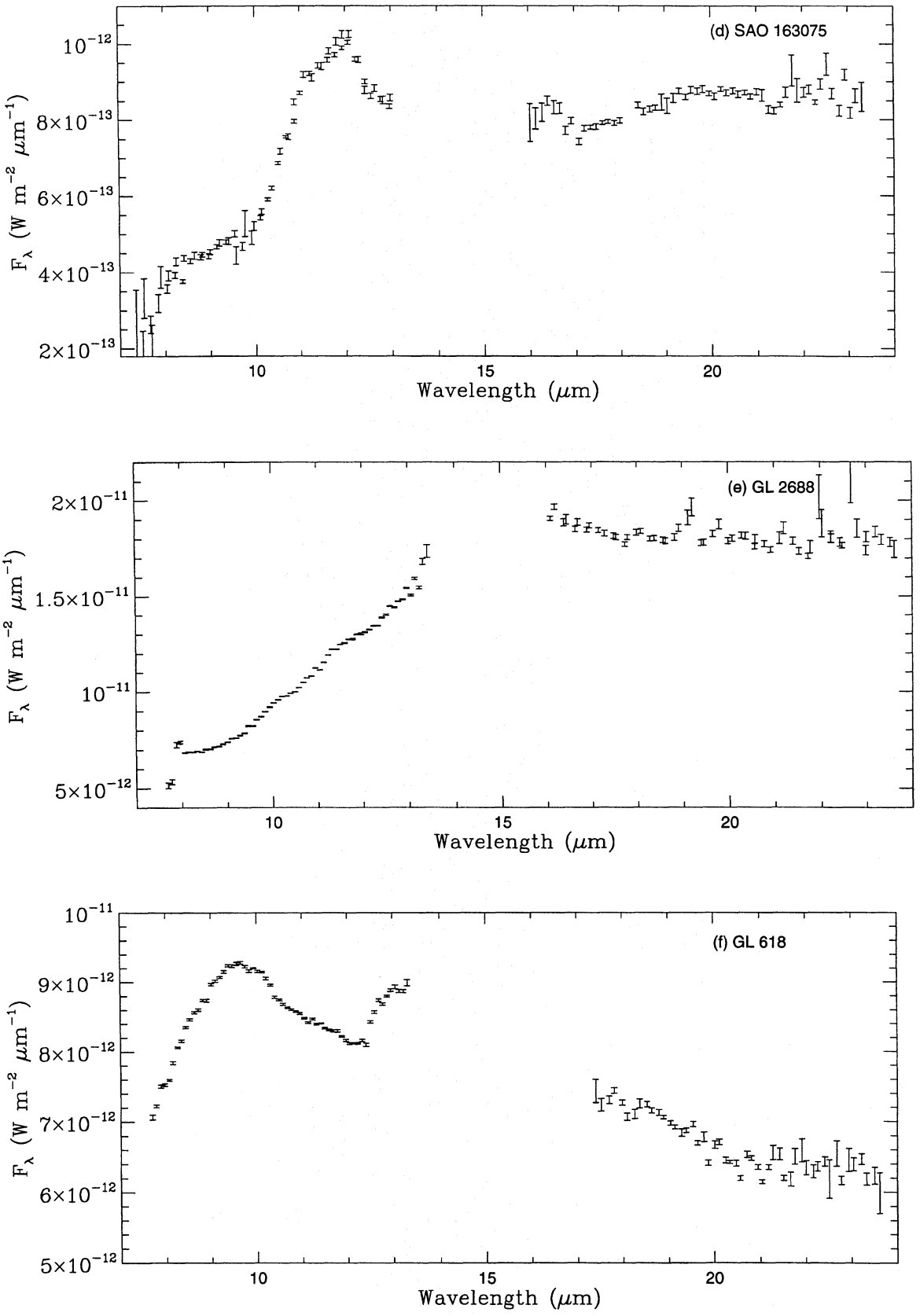

Fig. 2a–h. (continued)

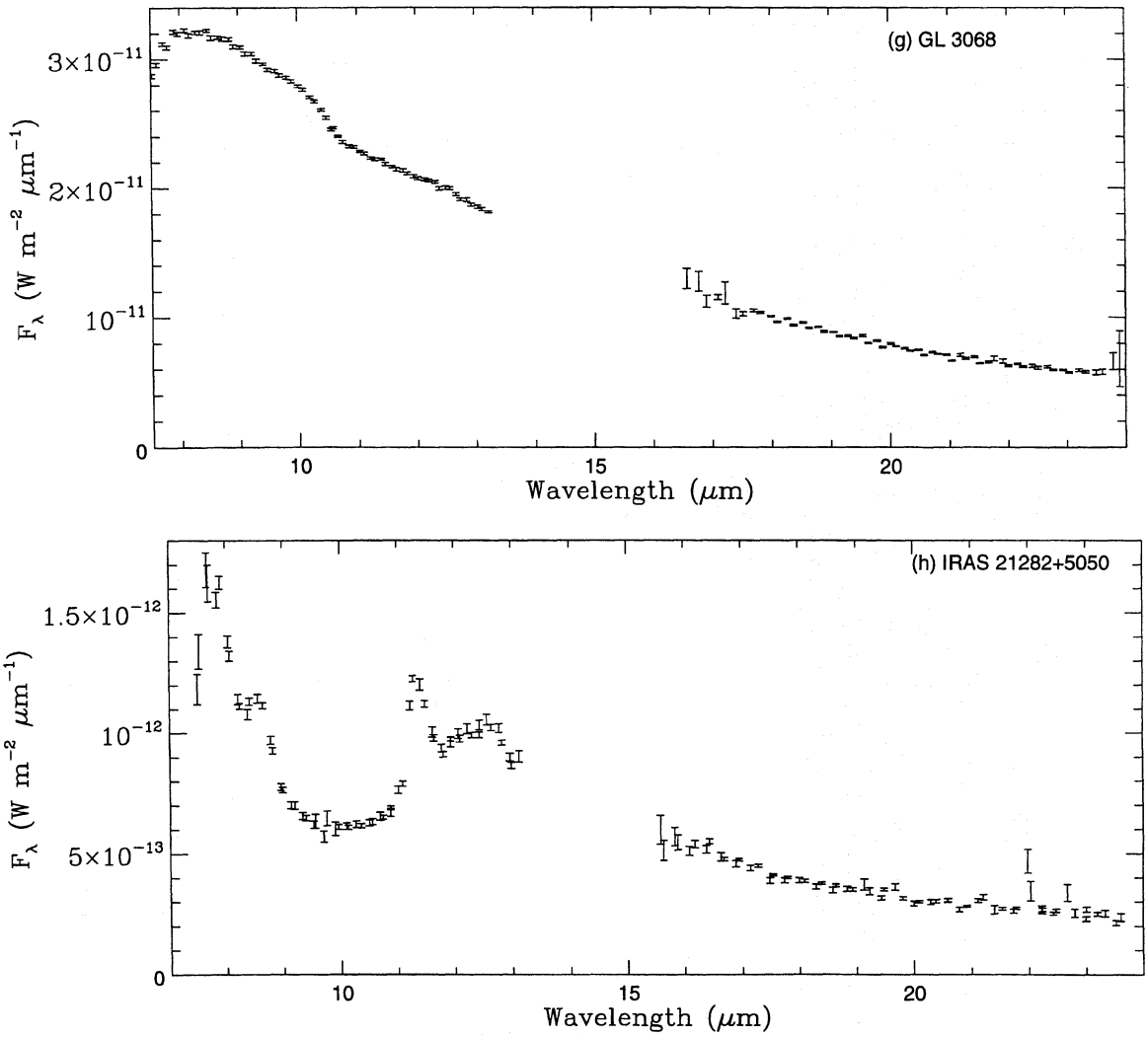

Fig. 2a–h. (continued)

Table 1. Sources observed

Source	Other names	Sp. type	Observation
IRAS 04296+3429		G0Ia	10 μm : 7/90 (UCLS) 10&20 μm : 10/90 (CGS3) 10.7&12.1 μm (hi-res): 10/90 (CGS3)
GL 618	IRAS 04395+3601	(B0)	10&20 μm : 11/93 and 10/90 (CGS3)
IRAS 05341+0852		F:	10 μm : 12/90 (UCLS)
IRAS 07134+1005	SAO 96709; HD 56126	F5I	10&20 μm : 5/91 (CGS3)
He 2–447	IRAS 19431+2112	PN	10 μm : 7/90 (UCLS)
SAO 163075	IRAS 19500–1709; HD 187885	F3I	10&20 μm : 5/91 and 6/92 (CGS3)
GL 2688		F5Iae	10 μm : 7/90 (UCLS) 10&20 μm : 10/93 and 5/91 (CGS3)
IRAS 21282+5050		PN	10&20 μm : 5/91 (CGS3)
IRAS 22272+5435	SAO 34504; V354 Lac; HD 235858	G5Ia	10 μm : 7/90 (UCLS) 10&20 μm : 10/90 (CGS3)
GL 3068	IRAS 23166+1655	C	10&20 μm : 10/90 (CGS3)

Note: Circular apertures of 4.5 arcsec and 5.5 arcsec diameter were respectively used for the UCLS and CGS3 spectra, except for the CGS3 10 μm spectrum of GL 2688, for which a 9 arcsec circular aperture was used

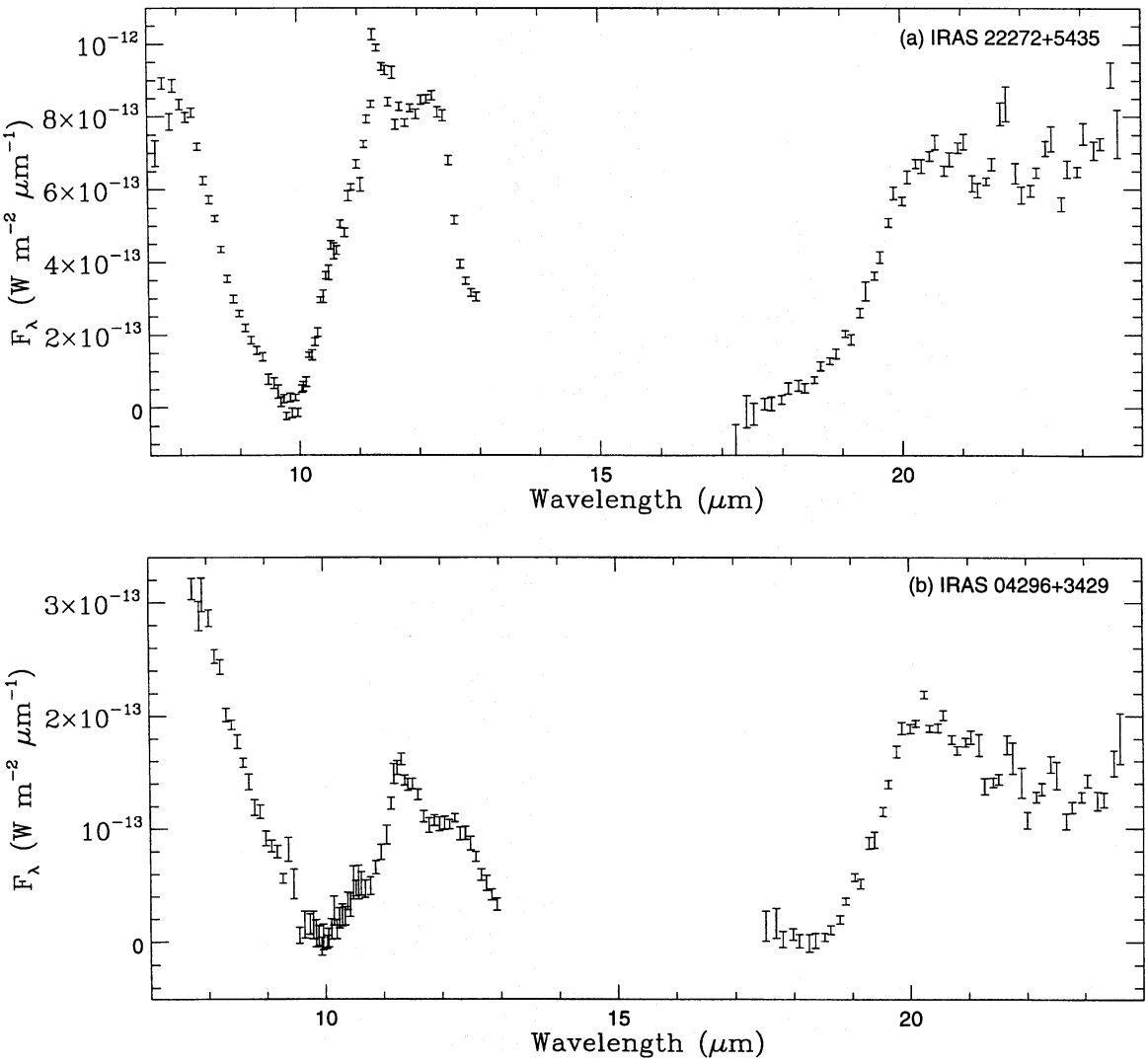

Fig. 3a–d. The excess spectra of four 21-μm band sources after subtraction of blackbodies normalised to 10.0 and 18.0 μm (see text). This allows the various features to be more clearly discerned, particularly in the case of SAO 163075. **a** IRAS 22272+5435; **b** IRAS 04296+3429; **c** IRAS 07134+1005; **d** SAO 163075

The spectra are clearly different from the standard UIR spectrum, but the rise towards the short wavelength end of our spectra appears to be be due to the long-wavelength wing of the 7.7 μm UIR feature, displaced towards somewhat longer wavelengths than usual: 7.94 μm in the case of IRAS 22272+5435 and 04296+3429 (Table 2). These two objects also exhibit rather weak subsidiary peaks in the red wing of this feature, at 8.2 μm and at 8.5–8.6 μm respectively (Table 2), the latter perhaps associated with the usually fairly strong 8.65 μm feature seen in standard UIR spectra. Buss et al. (1990), using airborne spectra that extended to shorter wavelengths, have argued that in the case of the 21-μm band objects, the 7.9 μm feature, normally much stronger than an underlying 6–9 μm plateau in standard UIR spectra, is dwarfed by the underlying 6–9 μm plateau.

The emission peaks measured at 11.3 μm (Table 2) are presumably associated with the strong, narrow 11.25 μm UIR band although they are unusually broad. A new, but weak, feature is present at 10.6 μm in the spectra of IRAS 04296+3429, 07134+1005 and 22272+5435, and their spectra also show new peaks at 11.5 μm and 12.23 μm (Table 2), on top of a broad underlying plateau of emission. Sylvester, Barlow & Skinner (1993) have detected the 10.6-μm emission feature amongst the family of of UIR-bands that are found superposed upon the silicate emission profiles of a number of luminous M supergiants. Our higher resolution (R = 200) 10 μm spectrum of IRAS 04296+3429 shows its 10.6-μm feature to be unresolved, implying a FWHM of $\leq$ 0.10 μm.

The sources can be arranged in a sequence of increasing departure from the standard UIR spectrum. IRAS 05341+0852 (Fig. 1e) has a prominent feature peaking near 11.25 μm that is significantly broader than the standard UIR 11.25-μm band, and a flat emission plateau extending to about 12.5 μm. IRAS

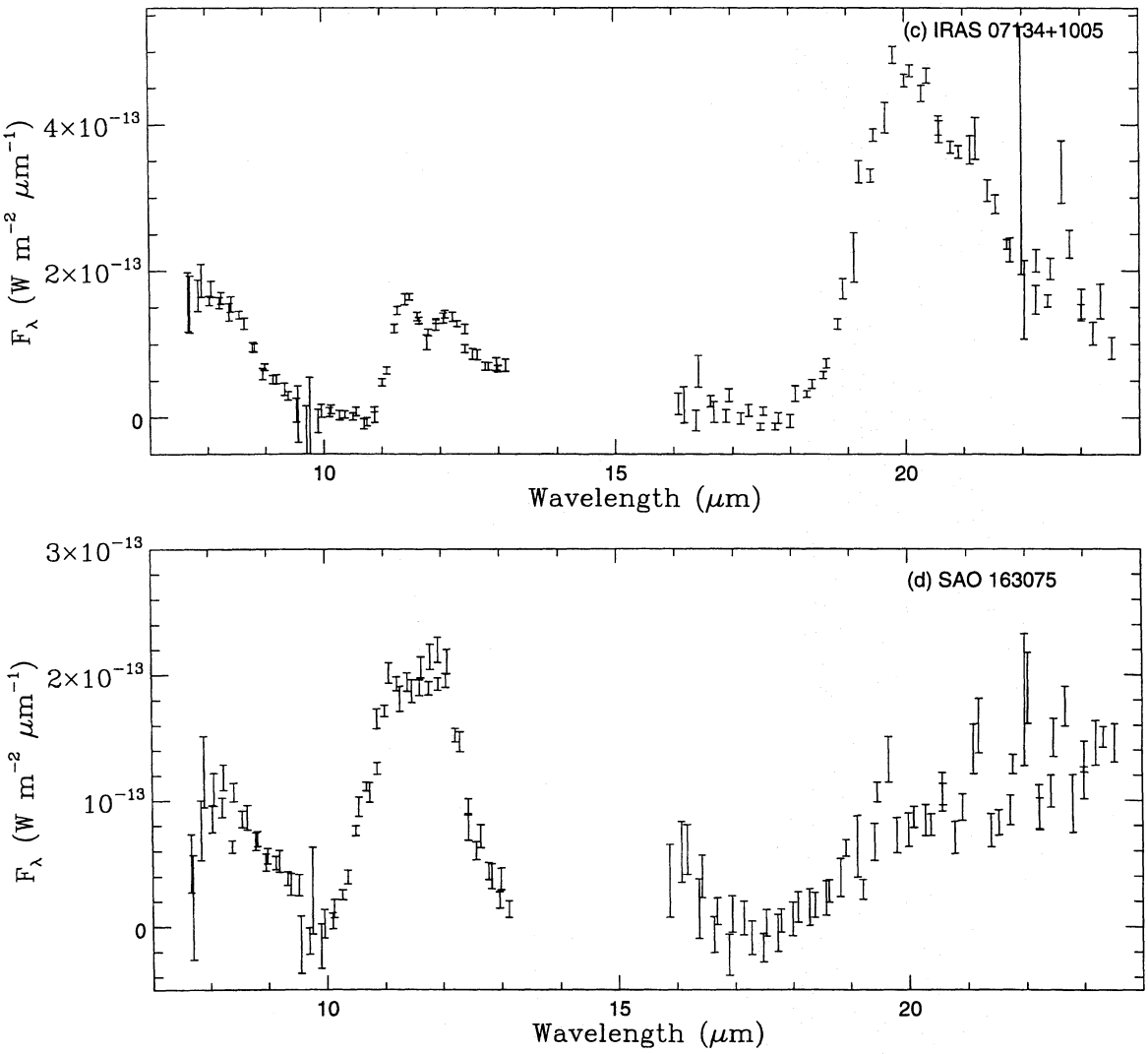

Fig. 3a–d. (continued)

04296+3429 (Fig. 1b) also has a prominent 11.3-μm band, which appears to have a narrow core and a broad red wing on which a subsidiary peak at 11.5 μm is superposed, plus a strong plateau which falls away beyond 12.4 μm, with another peak at 12.23 μm, and a weak feature near 10.6 μm. IRAS 22272+5435 (Fig. 1a) has a clear 11.3-μm band, again with a pronounced red wing and subsidiary peak at 11.5 μm, a stronger peak at 12.2(3) μm and a weak feature near 10.6 μm. In the spectrum of IRAS 07134+1005 (Fig. 1c) the peak at 12.2(3) μm is higher than the 11.3-μm peak; the plateau also has a sharper blue edge, rising abruptly at 11 μm – the component of the plateau upon which the 10.6-μm feature is superposed in the case of IRAS 22272+5435 and 04296+3429 appears to be largely absent in the case of IRAS 07134+1005. The spectrum of SAO 163075 (Fig. 1d) is dominated by an emission peak near 12 μm with at most only a weak 11.3-μm band. It also has a weak feature at 10.6 μm. The excess spectra plotted in Fig. 3 show that the strength of the 11–13 μm complex is less than that of the 8–9 μm complex in the case of IRAS 04296+3429, comparable in the the case of IRAS 22272+5435 and 07134+1005, and significantly stonger in the case of SAO 163075.

3.3. Emission features in the 20-μm spectra of post-AGB sources

Spectra at 16–24μm were obtained for a number of the post-AGB objects. A strong, broad emission band rises sharply from 18 to 20 μm in three of the objects, IRAS 07134+1005, 22272+5435 and 04296+3429. This feature was discovered in the *IRAS* LRS spectra of these sources by Kwok et al. (1989), who dubbed it the '21 micron feature'. Our 20-μm spectrum of SAO 163075 (Fig. 2d) appears to show the 21-μm feature very weakly in emission, making this source an addition to the small group of objects so far found to exhibit the 21-μm feature. In the spectra presented in Figs. 2 and 3, the 21-μm band actually peaks much closer to 20 μm than to 21 μm; it is likely that the combination of the steeply rising continua towards longer wavelengths and the relatively low spectral resolution of the

IRAS LRS combined to shift the apparent peak longwards. In the three objects where the 21-μm band is prominent (Figs. 2a-c), the short wavelength edge of the feature appears to follow the same profile; in contrast the profile of the long wavelength wing varies substantially, which may be influenced by varying contributions from the broad 30 μm emission bands seen in these objects (Omont 1993; Cox 1993).

In the case of the two G-type post-AGB sources in our sample, IRAS 04296+3429 and 22272+5435, the extended long wavelength wing of the 21-μm band apparently exhibits at least five subsidiary peaks (see Fig. 2). The 20 micron atmospheric window contains a plethora of deep narrow absorption bands, mostly from water vapour, and variations in the water column or small instrumental wavelength shifts between the target and standard star could compromise correction for these atmospheric features and thus produce spurious structure. We have carefully checked our target and standard star raw spectra and cannot find convincing evidence for this. For example, the 20 μm spectrum of IRAS 04296+3429 was divided by and calibrated by a 20 μm spectrum of α Tau obtained immediately afterwards, at virtually the same airmass (1.07 versus 1.03 airmasses, respectively). The raw spectrum of α Tau shows transmission peaks at 20.144, 21.513, 22.270 and 22.803 μm that match well transmission peaks at 20.137, 21.517, 22.269 and 22.800 μm in a synthetic LOTRAN transmission spectrum (Rothman et al. 1987) calculated for Mauna Kea's altitude; these transmission peaks differ in wavelength from the observed peaks in our calibrated spectra of IRAS 22272+5435 and 04296+3429 (see below). Similarly, the troughs in the α Tau and LOTRAN transmission spectra do not match up in wavelength with the troughs in the calibrated spectra of the above two 21-μm band sources. We also experimented by dividing the raw 20 μm spectrum of IRAS 04296+3429 by that of the standard star β And, obtained at a similar airmass (1.04) but two hours earlier. The subpeaks in the 21-μm band persisted, whereas the 20 μm spectrum of GL 3068 (Fig. 1g), which was calibrated by the same β And spectrum, is completely featureless.

The observed sub-peaks in our CGS3 spectra of IRAS 22272+5435 and 04296+3429 are at 19.03, 19.35 (a shoulder), 19.88, 20.23, 20.59, 21.03, 21.72, 22.41 and 23.06 μm. These 21-μm band sub-peaks seen in our UKIRT spectra appear also to be present at the same wavelengths in the mean *IRAS* LRS spectrum of IRAS 22272+5435 (see e.g. Buss et al. 1990; their Fig. 3), which is not affected by the troublesome atmospheric bands that can sometimes afflict ground-based observations (the 20-μm region LRS spectrum of IRAS 04296+3429 is of too low signal-to-noise to be able to discern any substructure). The LRS database contains five separate long-wavelength region spectra of IRAS 22272+5435, all of which are of good signal-to-noise and exhibit excellent interagreement. In the mean LRS spectrum, sub-peaks in the 21-μm emission band are found at 19.88, 20.43, 21.03, 21.80 and 22.38 μm. The wavelengths of the LRS peaks at 19.88, 21.03, 21.80 and 22.38 agree reasonably with the CGS3 peak wavelengths at 19.88, 21.03, 21.72 and 22.41 μm; the peak at 23.06 μm seen in our CGS3 spectra is beyond the long-wavelength limit of the LRS spectrometer; while the *IRAS* LRS spectrometer would not have had sufficient resolution to resolve apart peaks at 20.24 and 20.59 μm, so the LRS peak at 20.43 μm could be consistent with the CGS3 peaks at 20.23 and 20.59 μm.

Barlow (1993) has suggested that the sub-peaks could be overtones of a 21-μm feature, since the spacings between the bands are roughly equal in frequency space (about 12 cm^{-1}). Dr. A. S. Webster (private communication) has suggested that they could arise from partially hydrogenated fulleranes, in particular 'magic species' such as $C_{60}H_m$, where $m = 12, 24, 36, 48$ and 60 (see Sect. 5.2). Further observations, particularly with ISO, are required to provide definitive spectra and determine the reality of these features.

We have taken the ratio of fluxes at the peak of the 21-μm feature (20.0 μm) to the continuum at 18.0 μm as a measure of the strength of the '21-μm feature', and list this quantity in Table 3. The feature is seen in objects with spectral types ranging from G8 (see the LRS spectrum of IRAS 20000+3239, Kwok et al. 1989) to F3 (SAO 163075, this paper), but reaches maximum prominence in the middle of this range (in IRAS 23304+6147, IRAS 04296+3429 and particularly IRAS 07134+1005, which are of spectral types G2Ia, G0Ia and F5I respectively). It seems that the 21-μm band is produced in the circumstellar envelopes of post-AGB objects spanning only a narrow range of spectral types and attains maximum prominence near the middle of that range.

3.4. Absorption features in the spectra of the C-rich sources GL 618 and GL 3068

In Figs. 1(g) and 1(h), and in Figs. 2(f) and 2(g), we show the 10 and 20 μm spectra of two heavily obscured carbon-rich objects in which absorption bands appear that may be related to the emission features discussed above. The 8–24 μm spectrum of the post-AGB object GL 618 shows a broad depression between 10 and 13 μm, together with a weaker minimum near 20 μm and a turnover below 9 μm. The absorptions appear to mirror the emission features seen in the sources that display the 21-μm band, corresponding to the broad 12 μm peak and the 21-μm band [1]. The spectrum of the highly evolved carbon star GL 3068 is less extreme, but it too shows evidence of a broad absorption band in the 10.5–13 μm region together with a turn-over near 8 μm. These 10.5–13 μm absorption bands have previously been interpreted as being due to absorption by SiC grains (Lequeux & Jourdain de Muizon 1990 for GL 618; Jones et al. 1978 for GL 3068). We have extracted the absorption profiles of these features by normalising blackbodies to the continuum points at 9 and 13 μm and then dividing the observed spectra into these

[1] We considered the alternative possibility that a silicate emission feature gives rise to the broad peak centred at about 9.6 μm in Fig. 1(g), but this hypothesis would leave unexplained the sharp rise in flux that begins at at about 12.4 μm, seen in both our spectrum and in the *IRAS* LRS spectrum The fact that a 265 K blackbody when normalised at 8 μm to the spectrum plotted in Fig. 1(g) passes exactly through the spectral points longwards of 13 μm provides further evidence that the drop in flux between 9.6 and 13 μm is due to an absorption feature.

Table 2. Peak wavelengths of emission features seen in the 10 μm spectra of 21-μm band sources

Band peak wavelengths[a] (μm)					PAH assignment
IRAS 22272	IRAS 04296	IRAS 07134	Chrysene	UIR-bands	
				7.7	C=C stretch
7.94	7.94	8.0–8.3	7.91		
8.2	8.2(s)	"	8.12	–	
8.6(s)	8.5(s)	?	–	8.65	C-H in-plane bend
10.6(s)	10.6(s)	10.6(s)	10.6	–	
11.3	11.3	11.3(s)	11.3	11.25	C-H out-of-plane bend for non-adjacent H-atoms
11.5(s)	11.5(s)	11.5	11.5	–	
–	–	–	–	11.9	C-H out-of-plane bend for doubly adjacent H-atoms
12.2(3)	12.2(3)	12.2(3)	12.2	–	
–	–	–	–	12.7	C-H out-of-plane bend for triply adjacent H-atoms

[a] 's' = shoulder on stronger feature

Table 3. 20 μm to 18 μm flux ratios measured for the 21-μm band objects

Source	Spectral type	$F_\lambda(20\mu m)/F_\lambda(18\mu m)$	Comment
IRAS 20000+3239	G8Ia	1.24	*IRAS* LRS spectrum
IRAS 22272+5435	G5Ia	1.41	CGS3 spectrum
IRAS 23304+6147	G2Ia	2.06	*IRAS* LRS spectrum
IRAS 04296+3429	G0Ia	1.85	CGS3 spectrum
IRAS 07134+1005	F5I	2.28	CGS3 spectrum
SAO 163075	F3I	1.05	CGS3 spectrum

blackbodies; this yields the absorption profiles in 'emission' (Fig. 4).

The absorption profile for GL 3068 is derived from a continuum represented by a 380 K blackbody curve and shows an asymmetric profile with an extended red wing (Fig. 4a). It peaks near 11 μm, has a FWHM of 1.6 μm, and closely resembles the SiC profile seen in emission in carbon stars and planetary nebulae (see Sect. 3.1). A 265 K blackbody curve fitted to the spectrum of GL 618 at 8 μm provides an excellent fit to the prominent rise between 8 and 9.5 μm, as well as to the continuum points longwards 13 μm. The derived absorption profile (Fig. 4b) peaks near 12 μm with an asymmetry in the opposite sense to that derived for GL 3068, has a FWHM of 2.3 μm and a FWZI of 3.9 μm, and a peak optical depth of 0.17. The profile of the absorption feature in the spectrum of GL 618 more closely resembles the broad 10–13 μm emission complex seen in the spectra of 21-μm feature sources than does the profile derived from the absorption feature in the spectrum of GL 3068. While SiC appears to be responsible for the GL 3068 absorption feature and may make a small contribution to the broader absorption feature seen in the spectrum of GL 618, the fact that the absorption of laboratory samples of SiC peaks between 11.1 and 11.4 μm (Friedemann et al. 1981; Borghesi et al. 1985) leads us to conclude that SiC is not the dominant material responsible for the GL 618 absorption feature, which peaks near 12 μm.

In Figs. 5(a-d) we compare the observed GL 618 absorption profile (plotted in emission, as discussed above) with the 8–13 μm excess emission profiles that we derived for four 21-μm band sources. The GL 618 profile has been normalised to the top of the 12 μm plateau in each case. We see that the GL 618 profile provides a good match to the red side of the 10–13 μm emission complex, particularly in the case of IRAS 22272+5435 and 04296+3429 (Figs. 5a and 5b). The blue side of the 10–13 μm emission complex of these two sources is about 0.3 μm narrower than the GL 618 profile, but with a similar shape. As remarked in Sect. 3.2, in the case of IRAS 07134+1005 (Fig. 1c) the blue side of the complex is even narrower – the strong extended component upon which the weak 10.6 μm feature is superposed in the case of the other sources is completely absent here.

We conclude that whatever material is responsible for the 10–13 μm emission complex in the spectra of the 21-μm band sources is also responsible for the 10–13 μm absorption feature seen in the spectrum of GL 618. The 11.3-μm UIR-band feature is not seen in absorption in the GL 618 spectrum and must clearly have a different origin from the rest of the 10–13 μm complex. It is interesting to note that there appears to be a broad dip peaking at about 20–21 μm in the spectrum of GL 618 (Fig. 2f), although a better quality spectrum would be desirable. Given the similarity demonstrated above between the profile of GL 618's 10–13 μm absorption feature and the emission features at the corresponding wavelengths in the spectra of the 21 μm band sources, it seems reasonable to suggest that the 21 μm band itself is present, in absorption, in the spectrum of GL 618.

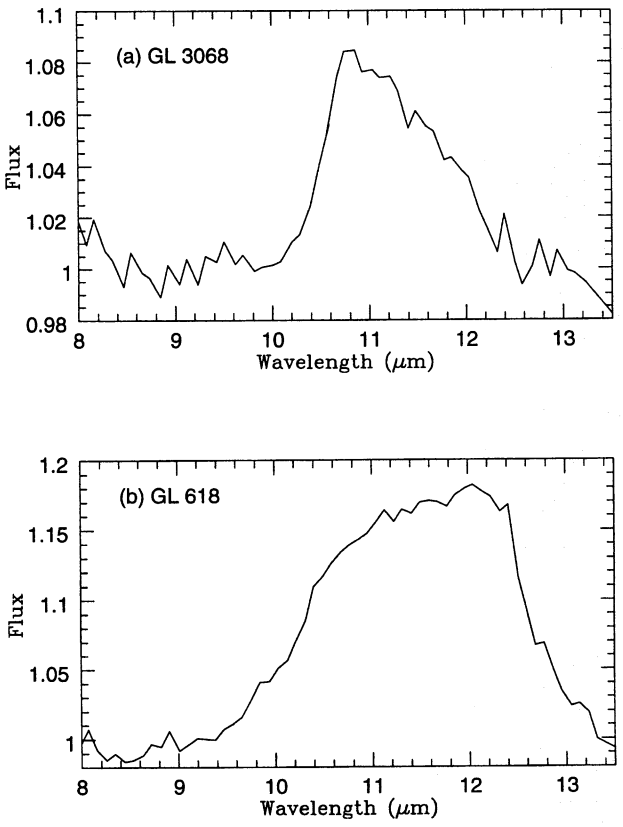

Fig. 4a and b. The absorption profiles observed towards GL 3068 and GL 618, plotted in 'emission'. These profiles were obtained by dividing the observed spectra into blackbodies that were normalised to the observed continuum levels at 9 and 13 μm. **a** GL 3068 after division into a 380 K blackbody. **b** GL 618 after division into a 265 K blackbody

For GL 618, the product of the peak optical depth of the 12-μm absorption feature (0.17) times the feature FWZI of 3.9 μm is 0.66 μm. Lequeux & Jourdain de Muizon (1990) detected a broad 3.4–3.5-μm absorption feature in the spectrum of GL 618, the product of whose peak optical depth (0.09) times FWZI (0.23 μm) is equal to 0.021 μm, a factor of 30 smaller than found for the 12-μm absorption band. This ratio of 30 is similar to the mean value of 30 found for the ratio of the integrated cross-section in the 11.3–11.9 band to that in the 3.3-μm band for a number of large compact PAH molecules (Leger et al. 1989). However, this may be coincidental, since the 11.3 and 3.3 μm bands are normally attributed to aromatic transitions, whereas the 3.4 μm band is attributed to aromatic overtones and/or aliphatic sidegroup transitions.

3.5. The spectrum of GL 2688

Figures 1(f) and 2(e) show that the 10 and 20 μm spectra of GL 2688, a bipolar post-AGB object with an F5Iae central star, is dominated by a strong continuum lacking sharp features. However, it does show evidence of an upturn from 9 to 7.8 μm, and two weak broad emission features extending between 9.5–10.5 and 10.5–12.2 μm. A UCLS 10 μm spectrum of GL 2688 taken in July 1990 also shows these features. There is no evidence in our spectra of a feature near 8.8 μm as claimed by Buss et al. (1993).

GL 2688 is unusual amongst the cool carbon-rich post-AGB objects in exhibiting only a 3.3 μm UIR-band feature (Geballe et al. 1992), with no longer-wavelength UIR-band features being detectable. Skinner et al. (1996) have attributed this behaviour to two effects: (a) the continuum of GL 2688 at 11 μm is about a thousand time stronger than at 3 μm, which would significantly reduce the contrast of the longer-wavelength bands if they had their usual flux ratios relative to the 3.3-μm band; (b) the dust optical depths derived by Skinner et al. for the equatorial torus of GL 2688 are very large, ~6 at 3.3 μm, ~2 at 10 μm, and ~50 for the UV/blue photons believed to be responsible for exciting the UIR-bands. They concluded that the observed 3.3-μm band photons are emitted at the inner edge of the torus and then scattered towards us by grains in the reflection lobes (so that the observed 3.3-μm feature should be significantly polarised), whereas the *scattering* optical depths of the reflection lobes at longer wavelengths are much smaller, so that the longer wavelength UIR-bands would not be seen in reflection.

4. The 7.5–13-μm spectra and the role of chrysene

The standard mid-infrared UIR-bands (column 5 of Table 2) are usually attributed to hydrogenated aromatic structures. No single species provides a match to the observed features but the wavelengths of the standard bands are sufficiently similar to those of amorphous carbon surface functional groups (Duley & Williams 1981) and, in particular, to those of polycyclic aromatic hydrocarbons (ATB89, Leger et al. 1989) for generic assignments to have been proposed (column 6 of Table 2).

The only one of the standard UIR-bands which is prominent in the spectra of the various post-AGB objects shown in Fig. 1 is the well-known feature at 11.3 μm, usually attributed to a C-H out-of-plane bend mode of isolated attached H-atoms. As listed in Table 2, three of the 21-μm band sources observed by us exhibit mid-infrared emission features that have not previously been observed as part of the standard suite of mid-infrared UIR-bands. The measured peak wavelengths of the new features are at 7.9, 8.2, 10.6, 11.5 and 12.2 μm. Remarkably, all of these wavelengths show a very good correspondence with the wavelengths of the main mid-infrared vibrational features measured by Cyvin et al. (1982) for one particular PAH molecule, namely chrysene ($C_{18}H_{12}$). The principal vibrational bands measured for this molecule by Cyvin et al. are illustrated by ATB85,89 for a number of excitation conditions. The strongest in-plane vibrational modes of chrysene are at 7.70, 7.90, 7.94, 11.51, 12.30 and 13.16 μm (Table 4 of Cyvin et al.), with weaker features measured at 8.12 and 8.75 μm, while the strongest out-of-plane bending modes of chrysene are found at 10.60, 12.20 and 13.4 μm, with the 10.6-μm band measured to be somewhat weaker than the latter two features (Table 6 of Cyvin et al.). Thus chrysene appears to provide a good match to the new peaks observed in the 7.5–13 μm spectra of the 21-μm band sources, if we

add to it a component (varying from source to source) which is responsible for the 'standard' mid-infrared UIR-bands, namely those at 11.3, 8.6 and 7.7 μm, as well as a very strong 10–13 μm emission plateau, which significantly reduces the contrast of the peaks.

Dr. Scott Sandford (NASA-Ames) has kindly made available to us a laboratory absorption spectrum measured at room temperature for chrysene in a KBr pellet. We have inverted this spectrum to obtain a pseudo-emission spectrum and then gaussian-smoothed this to resolutions of 0.09 and 0.18 μm, the same respectively as were used in obtaining the spectra of IRAS 22272+5435 and 04296+3429 that are plotted in Figs. 1(a) and (b). A comparison between the resulting spectra of chrysene and those of the two sources is shown in Figs. 6(a) and (b). We believe that this comparison supports the identification of the new astronomical features with chrysene, provided two factors are taken into account – (1) the very strong plateau emission present throughout the astronomical spectra, particularly in the 10–13-μm region, considerably diluting the contrast of discrete emission peaks; (2) the fact that the chrysene spectrum plotted in Fig. 6 was taken in absorption at $\sim$300 K, whereas ATB89 (e.g. their Fig. 13, which treats the case of chrysene) have shown how fluorescent emission excitation cascades in astronomical environments are likely to enhance the strength of shorter wavelength features relative to those at longer wavelengths.

Figure 6 shows a strong chrysene peak at 13.2 μm, beyond the long-wavelength edge of the two astronomical spectra that are plotted there. We only have one 10-μm region spectrum of a 21-μm band object which extends past 13 μm – the CGS3 spectrum of IRAS 22272+5435 illustrated in Fig. 2(a) – this appears to show a bump at about 13.2 μm, consistent with the expected chrysene peak. Chrysene also exhibits a noticeable peak at 9.7 μm (Fig. 6), In ground-based astronomical spectra, this unfortunately coincides with a strong atmospheric ozone absorption band which is notoriously difficult to correct for. Although the spectrum of IRAS 04296+3429 plotted in Fig. 6b and the spectrum of IRAS 22272+5435 plotted in Fig. 2a both exhibit apparent emission peaks at 9.7 μm, we are reluctant to claim that these are other than due to imperfect cancellation of atmospheric ozone absorption. Spectra obtained by ISO should be valuable in this respect.

The strongest IR vibrational bands of chrysene measured shortwards of 7.5 μm by Cyvin et al. (1982; see also Karcher et al. 1986 and Fig. 13 of ATB89) are C-C stretch modes at 6.97 and 6.27 μm, and C-H stretch modes around 3.3 μm (see Table 4 of Cyvin et al.). Buss et al. (1990) reported prominent emission bands at 6.9 and 6.2 μm in their *KAO* spectra of IRAS 07134+1005 and 22272+5435, while Geballe et al. (1992) found the latter object and IRAS 04296+3429 to exhibit strong 3.3-μm band emission, along with strong 3.4 and 3.5-μm band emission. The 6.9 μm emission band is unusual and is not one of the 'standard' astronomical UIR emission bands. Its presence is consistent with the chrysene identifications suggested above for the new features observed in the 7.5–13 μm region. Thus all of the strong vibrational features seen in the laboratory spectra of chrysene have counterparts in the infrared spectra of these C-rich post-AGB objects. No other PAH molecule in the large compilation of laboratory IR spectra by Karcher et al. (1986) provides as good a match to the observed peaks – several PAH molecules in their compilation can match some (but not all) of the observed peaks, but also predict bands where none are observed.

Prior to the discovery by Sylvester, Barlow & Skinner (1994) of mid-infrared UIR emission bands in the spectra of a number of luminous oxygen-rich M supergiants, the 21-μm band post-AGB objects were the coolest stars known to excite UIR-bands. Sylvester et al. were able to attribute the UIR-band emission from cool M supergiants to excitation by chromospheric UV photons, but the F–G type stars powering the 21-μm band sources are not thought to emit a significant flux of UV photons, chromospheric or otherwise. Buss et al. (1990) argued that the lack of UV photons and the presence of broad infrared features and plateaus in the spectra of the 21-μm band objects implied pumping by optical photons of large PAH clusters or HAC grains, because PAH clusters/HACs, to which they attributed the observed strong 6–9 μm and 11–13 μm plateaus, would be sufficiently large to efficiently absorb visible photons, whereas most molecular PAHs should absorb only weakly in the visible region.

If we assume that an assemblage of PAH molecules and clusters was present in the outflows around the immediate precursors to the 21-μm band sources, the above considerations suggest that as the central stars evolved to higher temperatures the first species to exhibit their infrared emission features would be those capable of absorbing the optical photons emitted by the central stars as they evolved to G- and then F-type, namely large PAH clusters, plus individual PAH molecules with absorption cut-ons in the optical rather than in the UV. However, the absorption cut-on of chrysene molecules is measured to be at $\sim$ 3250 Å (Karcher et al. 1986), not sufficiently longwards of that of other small PAH molecules to suggest that chrysene would be the first PAH molecule to be picked out from an assemblage of different molecules by a stellar radiation field that was gradually evolving to hotter G- and F-type temperatures. Thus if an identification for the new features with chrysene is valid, the above considerations would appear to suggest an enhanced abundance for chrysene, rather than a selective excitation mechanism. The disappearance of the new mid-infrared features as the post-AGB exciting stars evolve to earlier spectral types can be straightforwardly understood if the features are due to chrysene, since ATB89 (their Fig. 21) have shown that chrysene, $C_{18}H_{12}$, will be rapidly dehydrogenated upon absorption of photons with energies in excess of $\sim$10 eV (e.g. Lyman-α), whereas PAHs with more than 25-30 C-atoms should retain their full complement of H-atoms when exposed to radiation fields which extend as far as the Lyman limit (13.6 eV). During the later phases, dehydrogenated chrysene molecules would resemble the very small carbon grains ($\leq$10 Å radius) that have been invoked to provide (via temperature-spiking) the hot near-IR excess emission observed in the spectra of reflection nebulae (Sellgren 1984). Such hot near-IR excess emission is also present in the spectra of some

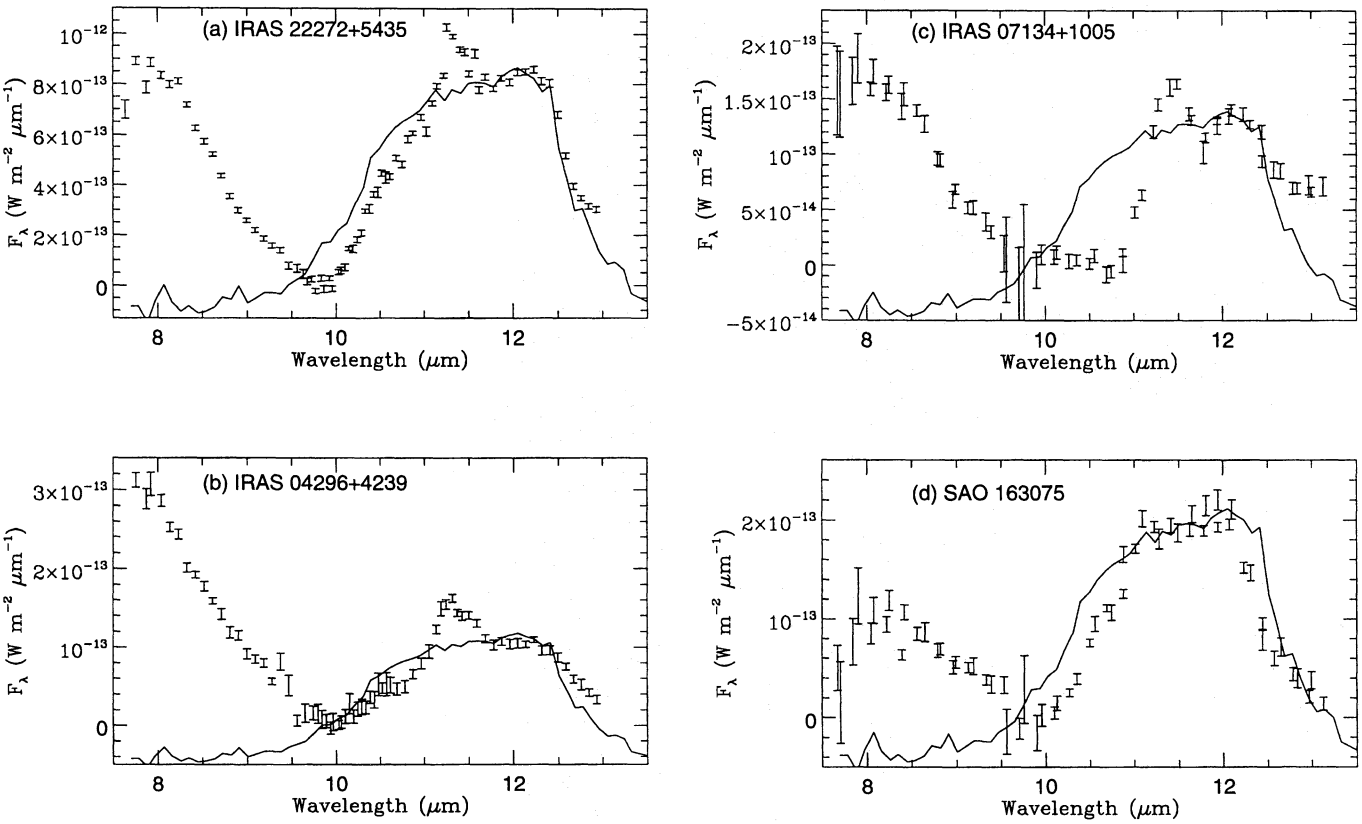

Fig. 5a–d. Comparison of the observed GL 618 absorption profile (solid line; plotted in 'emission', see text) with the 8–13-μm excess emission profiles derived for four 21-μm band sources. **a** IRAS 22272+5435; **b** IRAS 04296+3429; **c** IRAS 07134+1005; **d** SAO 163075

planetary nebulae. Thus any chrysene molecules present during the F/G supergiant phase ought to exist in a completely dehydrogenated state during the later, hotter phases of the central star evolution and should therefore not contribute to the overall C-H band emission by the PAH ensemble (e.g. the 3.3 and 11.3 μm bands) although they should continue to contribute to the C-C band emission (e.g. the 6.2 and 7.7 μm bands). This might help alleviate the discrepancy found Schutte et al. (1993), who, in order to match astronomical UIR-band spectra with theoretical PAH ensemble spectra, had to increase the strengths of the 6.2 and 7.7 μm bands, measured in laboratory spectra, by a factor of about five relative to those measured for C-H transitions.

5. Possible carriers of the 21-μm band

A variety of identifications have been proposed for the 21-μm band carriers. It may be useful to separate these into two categories: (a) inorganic materials; and (b) carbon-rich species. An important observational constraint that must be satisfied by any proposed identification is the apparent fragility of the 21-μm band carrier. The 21-μm band has never been observed in the spectra of AGB stars, in particular carbon stars, nor in the spectra of planetary nebulae. Its documented appearance is so far confined to post-AGB stars having a relatively narrow range of spectral types, from F3I to G8I (Hrivnak 1995).

5.1. Identifications of the 21-μm band with inorganic compounds

Goebel (1980) and Goebel & Moseley (1985) proposed solid MgS as the carrier of the strong 30-μm emission band that is observed in the spectra of carbon stars and C-rich PN – this 30-μm feature is also strongly present in emission in the spectra of the 21-μm band objects (Omont 1993; Cox 1993; the latter paper contains a listing of all sources then known to exhibit the 30-μm emission band). Using laboratory measurements of the optical constants of MgS particles, Begemann et al. (1994) were able to obtain agreement with the profile and peak wavelength of the astronomical 30-μm feature. Although carbon-rich compounds might be suspected to be responsible for the 30-μm feature, given the carbon-rich nature of the exciting stars and the presence of other carbonaceous features in their IR spectra, a convincing identification of the 30-μm feature with a carbon-rich material has yet to be made.

Goebel (1993) has proposed solid SiS_2 as the material responsible for the astronomical 21-μm emission band. He noted that solid SiS_2 exhibits an absorption feature peaking within 1 μm of the peak of the astronomical 21-μm band. The main problem that we perceive with this identification for the 21-μm band is that SiS_2 does not appear to be fragile enough to satisfy the observational constraints. MgS has a melting point

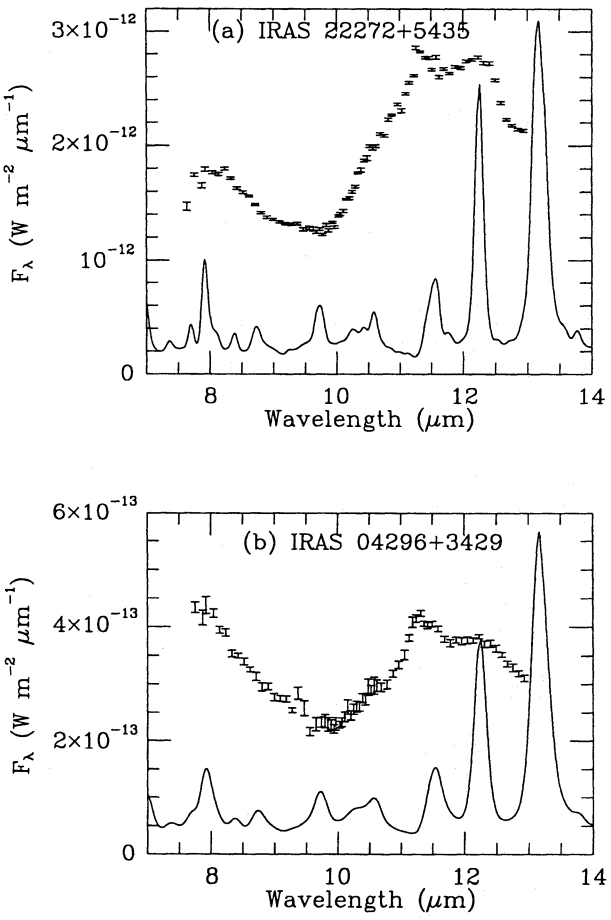

Fig. 6a and b. The spectra of **a** IRAS 22272+5435 and **b** IRAS 04296+3429, both plotted as error bars, are compared with a room-temperature laboratory spectrum of chrysene (solid line). The chrysene spectra that are plotted were obtained by inverting an absorption spectrum of chrysene (made available to us by Dr. Scott Sandford) and then convolving this to the same resolution as the astronomical spectra (0.09 μm FWHM in **a** and 0.18 μm in **b**) and renormalising to an appropriate flux level for the comparison

of $\geq$ 2300 K (Weast 1992) and the observed appearance of the 30-μm emission band, right through the evolutionary sequence from carbon stars to post-AGB objects and on to C-rich PN, is consistent with expectations for the robustness of MgS. SiS_2 has a sublimation temperature of $\sim$ 1400 K (Weast 1992), lower than that of MgS, but not particularly fragile. An identification with SiS_2 would not appear to explain the observed restriction of the 21-μm emission feature to post-AGB objects with spectral types in the narrow range F3–G8.

5.2. *Identifications of the 21-μm band with carbon-rich species*

Extremely strong (and unusual) C_2 and C_3 molecular absorption features are observed in the optical spectra of the F3I – G8I central stars of the 21-μm band objects (Hrivnak 1995), consistent with a large degree of self-enrichment in carbon by the 3rd dredge-up while the star evolved up the AGB. This, together with the definite presence in their spectra of the 11.3 μm emission band seen in many other carbon-rich environments and attributed to the C-H out-of-plane bending modes of PAH-like structures, plus the apparent identification of the other mid-infrared emission features observed in the spectra of the 21-μm band sources with the PAH molecule chrysene (Sect. 4), makes it natural to seek an identification of the 21-μm band itself with some carbon-rich species.

In their 21-μm band discovery paper, Kwok et al. (1989) noted that HNC, $[CNO]^-$ and NCO all have bending modes in the 20-μm region. Although the required abundance for HNC in a C-rich envelope is reasonable, the expected emission in other vibrational modes of this molecule is not observed, and Omont et al. (1993) have argued against HNC as the 21-μm band carrier on the basis of a deficiency of HCN in the millimetre-wave spectrum of IRAS 07134+1005. Sourisseau, Coddens & Papoular (1992) proposed that the 21-μm feature could be due to N-C-N and O-C-N deformation vibrations of simple amides, such as urea and thiourea, though a mechanism for the production of sufficient quantities of such species has not yet been suggested.

Most PAH molecules have ring deformation vibrational modes in the 20-μm region (Karcher et al. 1986, ATB89). The excellent correpondence found in Sect. 4 between the new bands in the 7.5–13-μm spectra of the 21-μm band sources and the vibrational modes of chrysene ($C_{18}H_{12}$) suggests that ring deformation modes of PAHs need to be seriously considered as responsible for the astronomical 21-μm emission band. Chrysene itself has no emission bands occurring between 15 and 18 μm and is measured to have medium and strong vibrational modes at 21.0 and 23.7 μm, respectively (Cyvin et al. 1982). Our spectra do not extend sufficiently far to encompass the latter feature, and athough one of the five apparent sub-peaks in the 21-μm band spectra of IRAS 22272+5435 and 04296+3429 lies at 21.03 μm (Sect. 3.3), it is clear that chrysene alone could not account for the whole of the observed 21-μm band profiles. However, given that so many different PAH molecule have ring deformation modes in this spectral region (Karcher et al. 1986), an appropriate ensemble of PAH species might be capable of accounting for the observed features.

IRAS 04296+3429 and IRAS 22272+5435, the two G-type sources with apparent subpeaks in their 21-μm band profiles, were found by Geballe et al. (1992) to have much stronger than normal 3.4-μm and 3.5-μm emision features relative to the 3.3-μm feature, whereas in the spectrum of IRAS 07134+1005, the F-type source whose 21-μm feature does not exhibit obvious subpeaks in its red wing, the 3.3-μm and 3.4-μm features have their more usual ratio (Kwok, Hrivnak & Geballe 1990). The strength of the 3.4 and 3.5-μm bands in the first two sources, relative to the 3.3-μm band, is too high to explained by 'hot-band' overtone emission (ATB89, Schutte Tielens & Allamandola 1993), and de Muizon et al. (1986) have argued that they are most likely to be due to aliphatic sidegroups (e.g. $-CH_3$) attached to PAH molecules (Duley & Williams 1981). Schutte et al. (1993) have proposed that the 3.4 and 3.5-μm bands may be due to superhydrogenated-PAHs (SPAHs), in which case one

might speculate that SPAHs might be responsible for the 21-μm feature too (chrysene ($C_{18}H_{12}$) is one of the most hydrogenated of the 'normal' PAH molecules, due to its non-condensed structure). Since all of the objects showing the 21-μm band are cool F/G-type stars, as well as most of the known sources with anomalously high flux ratios of the 3.4 and 3.5-μm bands relative to the 3.3 μm band, it could be speculated that when the exciting star gets hotter than F/G the PAH molecules and clusters are dehydrogenated and ionized, leading to the disappearance of the 21 μm band, a reduction in the strength of the mid-infrared 6–9-μm and 10–13-μm plateaus and a reduction in the strength of the 3.4 and 3.5-μm bands relative to the 3.3-μm band, plus a strengthening of the 'standard' UIR-bands, which in this picture would be due to ionized partially dehydrogenated PAHs. Thus by the time the central sources of post-AGB objects have evolved to A/B-types (e.g. HD 44179 or HR 4049), the degree of hydrogenation could be reduced sufficiently for the highly hydrogenated features to have disappeared, replaced by the 'standard' bands seen in hotter sources such as IRAS 21282+5050 and He 2–447, e.g. the 11.3-μm feature, which is believed to be produced by PAHs which have just one hydrogen atom per ring (Cohen, Tielens & Allamandola 1985).

The 3-dimensional analogues of the 2-dimensional PAH molecules are the fulleranes (hydrogenated fullerenes, Webster 1993), e.g. $C_{60}H_m$, based on the buckminsterfullerene molecule C_{60} (Kroto et al. 1985). Webster (1993) has calculated the predicted wavelengths for the infrared-active vibrational modes of $C_{60}H_{60}$. The main bands are predicted to occur at 3.43, 6.50, 7.00, 7.86, 8.83, 10.4, 20.5 and 23.0 μm. Six of these eight wavelengths are close to observed peaks in the spectra of the 21-μm band sources. A broad plateau in the 8-μm region was also predicted. Webster (1995) has extended these calculations to predict the wavelength of the lowest energy fullerane mode as a function of the number of attached H-atoms m. He finds the wavelength to be a strong function of m, increasing from 19 μm for m = 0 to 23 μm for m = 60, and that in each case the transition should be split over a wavelength range of about 1 μm. He notes that a mixed population of fulleranes is therefore likely to produce a broad band extending over the whole 19–23-μm range and suggests this as an identification for the astronomical 21-μm band. As noted in Sect. 3.3, Webster (private communication) has suggested that the apparent subpeaks observed by us in the spectra of two of the 21-μm band sources could correspond to particularly stable species, e.g. with m = 12, 24, 26, 48 and 60. If the suggested fullerane identification for the 21-μm emission feature is correct, the absence of the feature in the spectra of earlier-type post-AGB objects and PN could be due to the complete dehydrogenation and/or break-up of the fulleranes by that stage of evolution.

6. Conclusions

The mid-infrared spectra of the dust around the carbon-rich post-AGB stars discussed here display a number of intriguing features that give important clues to the composition of the dust and its relationship to the commonly-observed carbonaceous dust signatures seen in carbon stars and planetary nebulae and attributed to silicon carbide and aromatic hydrocarbon molecules.

1) 10-, and in most cases, 20-μm spectra of a sample of F- and G-type post-AGB stars are presented together with comparison spectra of the dust-shrouded objects GL 618, GL 3068 and GL 2688 and the planetary nebulae He 2-447 and IRAS 21282+5050.

2) The spectra of the optically-visible F- and G-type post-AGB stars, IRAS 05341+0852, 04296+3429, 22272+5435, 07134+1005 and SAO 163075 appear to form a sequence of increasing departure from the standard UIR band spectrum. A broad red wing increasingly dominates the narrow 11.25 μm UIR band, while a strong, broad emission complex spanning the 11-13 μm region becomes more and more prominent. The 21-μm emission band first identified by Kwok et al. (198) in *IRAS* LRS spectra is very pronounced in the middle objects in this sequence.

3) The peak of the 21-μm band lies very close to 20 μm. The feature is apparently confined to dust shells around post-AGB stars of spectral type G8I to F3I and attains maximum prominence near the middle of this range. The spectra of IRAS 22272+5435 and 04296+3429 display a series of subsidiary peaks at 20.2, 20.6, 21.0, 22.4 and 23.1 μm; if these peaks are real, they could be due to overtones of the 21-μm band. The 21-μm band could arise from skeletal vibrational modes of PAHs or from partially-hydrogenated fulleranes. We consider that it is likely that the 21-μm band is produced by highly-hydrogenated species that become dehydrogenated as the exciting star temperature increases.

4) The 11–13-μm emission complex shows discrete peaks at 10.6, 11.5 and 12.2 μm, which, together with additional weak features at 7.9 and 8.2 μm form a family of weaker emission bands analogous to the UIR emission features. The wavelengths of these weak additional bands, together with features at 6.2 and 6.9 μm reported by Buss et al. (1990) for two of the objects in this sample, are coincident with strong emission bands measured in laboratory spectra of the highly-hydrogenated PAH chrysene ($C_{18}H_{12}$). If the attribution of these weak features to chrysene is correct, then it would appear that the conditions in the dust shells around F- and G-type post-AGB stars lead to enhanced abundances of this PAH species, while the absence of these features in the UIR-band spectra of sources with hotter exciting stars is explainable in terms of the predicted complete dehydrogenation of the smallest PAH molecules by the UV radiation from these sources.

5) GL 618 and GL 3068 have thick dust shells that render them invisible and produce absorption bands in the 11–13-μm region. The absorption band profile extracted from GL 3068 closely resembles the SiC emission band seen in the spectra of planetary nebulae and carbon stars. However, the band profile extracted from GL 618 peaks at a significantly longer wavelength and is broader than the SiC band – its profile more closely resembles the broad 11–13-μm emission complex seen in the spectra of the F- and G-type post-AGB stars that display the 21-μm feature; the 21-μm feature appears to be present, but weakly in absorption, towards GL 618. It seems that the species that produce the complex emission spectra of the objects that display

the 21-μm emission band are also responsible for the absorption bands seen towards GL 618.

Acknowledgements. We thank Dr. Scott Sandford (NASA-Ames) for providing us with a digitised version of his laboratory spectrum of chrysene and Dr. Adrian Webster (ROE) for the communication of results in advance of publication. We are grateful to the staff at UKIRT for their excellent support. This work was supported, in part (CJS), under the auspices of the U.S. Department of Energy by Lawrence Livermore Laboratory under Contract No. W-7405-ENG-48. This work was performed while one of the authors (KJ) held a National Research Council-ARC Research Associateship.

References

Aitken D.K., Roche P.F., 1982, MNRAS 200, 217
Aitken D.K., Roche P.F., Spenser P.M., Jones B., 1979, ApJ 233, 925
Allamandola L.J., Tielens A.G.G.M., Barker J.R., 1985, ApJ 290, L25 (ATB85)
Allamandola L.J., Tielens A.G.G.M., Barker J.R., 1989, ApJS 71, 733 (ATB89)
Barlow M.J., 1983, in: Flower D.R. (ed.), Proc. IAU Symp. 103, Planetary Nebulae. Kluwer, Dordrecht, p. 105
Barlow M.J., 1993, in: Kwok S. (ed.). ASP Conf. Ser. Vol. 41, Astronomical Infrared Spectroscopy: Future Observational Directions. Astron. Soc. Pac., San Francisco, p. 97
Begemann B., Dorschner J., Henning T., Thamm E., 1994, ApJ 423, L71
Bond H.E., 1991, in: Michaud G., Tutukov A. (eds.). Proc. IAU Symp. 145,
Borghesi A., Bussoletti E., Colangeli L., De Blasi C., 1985, 153, 1
Buss Jr R.H., Cohen M., Tielens A.G.G.M., et al., 1990, ApJ 365, L23
Buss Jr R.H., Tielens A.G.G.M., Cohen M., et al. 1993, ApJ 415, 250
Cohen M., 1984, MNRAS 206, 137
Cohen M., Tielens A.G.G.M., Allamandola L.J., 1985, ApJ 299, L93
Cohen M., Allamandola L.J., Tielens A.G.G.M., et al., 1986, ApJ 302, 737
Cohen M., Tielens A.G.G.M., Bregman J., Simpson J.P., Witteborn F.C., Rank D., Allamandola L.J., Wooden D., de Muizon M., 1989, ApJ 341, 246
Cox P., 1993, in: Kwok S. (ed.). ASP Conf. Ser. Vol. 41, Astronomical Infrared Spectroscopy: Future Observational Directions. Astron. Soc. Pac., San Francisco, p. 163
Cyvin B.N., Klaeboe P., Whitmer J.C., Cyvin S.J., 1982, Z. Naturforschung, 37a, 251
de Muizon M., Geballe T.R., d'Hendecourt L.B., Baas F., 1986, ApJ 306, L105
Duley W.W., Williams D.A., 1981, MNRAS 196, 269
Fernie J.D., 1983, ApJ 265, 999
Friedemann C., Gurtler J., Schmidt R., Dorschner J., 1981, Ap&SS 79, 405
Geballe T.R., Tielens A.G.G.M., Kwok S., Hrivnak B.J., 1992, ApJ 387, L89
Geballe T.R., van der Veen W.E.C.J., 1990, A&A 235, L9
Gillett F.C., Forrest W.J., Merrill K.M., 1973, ApJ 183, 87
Goebel J.H., 1980, BAAS, 14, 858
Goebel J.H., 1993, A&A 1993, 278, 226
Goebel J.H., Moseley S.H., 1985, ApJ 290, L35
Hrivnak B.J., 1995, ApJ 438, 341
Hrivnak B.J., Kwok S., 1991, ApJ 371, 631
Hrivnak B.J., Kwok S., Geballe T.R., 1994, ApJ 420, 783
Hrivnak B.J., Kwok S., Volk K.M., 1989, ApJ 346, 265
Jones B., Merrill K.M., Puetter R.C., Willner S.P., 1978, AJ 83, 1437
Karcher W., Fordham R.J., Dubois J.J., Glaude P.G.J.M., Ligthart J.A.M., 1985, Spectral Atlas of Polycyclic Aromatic Compounds, Vols. 1 & 2, Reidel, Dordrecht
Kroto H.W., Heath J.R., O'Brien S.C., Curl R.F., Smalley R.E., 1985, Nat 347, 354
Kwok S., Hrivnak B.J., Geballe T.R., Langill P.P., 1993, in: Kwok S. (ed.). ASP Conf. Ser. Vol. 41, Astronomical Infrared Spectroscopy: Future Observational Directions. Astron. Soc. Pac., San Francisco, p. 123
Kwok S., Volk K.M., Hrivnak B.J., 1989, ApJ 345, L51
Leger A., Puget J.L., 1984, A&A 137, L5
Leger A., d'Hendecourt L., Défourneau D., 1989, A&A 216, 148
Lequeux J., Jourdain de Muizon M., 1990, A&A 240, L19
Likkel L., Forveille T., Omont A., Morris M., 1991, A&A 246, 174
Little-Marenin I.R., 1986, ApJ 307, L15
Luck R.E., Bond H.E., Lambert D.L., 1990, ApJ 357, 188
Mathis J.S., Lamers H.J.G.L.M., 1992, A&A 259, L39
Merrill K.M., Stein W.A., 1976a, PASP, 88, 285
Merrill K.M., Stein W.A., 1976b, PASP, 88, 294
Omont A., 1993, in: Kwok S. (ed.). ASP Conf. Ser. Vol. 41, Astronomical Infrared Spectroscopy: Future Observational Directions. Astron. Soc. Pac., San Francisco, p. 87
Omont A., Loup C., Forveille T., te Lintel Hekkert ., Habing H., Sivagnanam P., A&A 267, 515
Roche P.F., 1989, in: Torres-Peimbert S. (ed.). Proc. IAU Symp. 131, Planetary Nebulae. Kluwer, Dordrecht, p. 117
Roche P.F., Aitken D.K., Smith C.H., 1991, MNRAS 252, 282
Rothman L.S., et al., 1987, Appl. Optics, 26, 4058
Russell R.W., Soifer B.T., Willner S.P., 1977, ApJ 217, L149
Schutte W., Tielens A.G.G.M., Allamandola L.J., 1993, ApJ 415, 397
Sellgren K., 1984, ApJ 277, 623
Skinner C.J., Meixner M., Barlow M.J., et al., 1996, A&A (in press)
Sourisseau C., Coddens G., Papoular R., 1992, A&A 254, L1
Sylvester R.J., Barlow M.J., Skinner C.J., 1993, MNRAS 266, 640
Trams N.R., Waters L.B.F.M., Lamers H.J.G.L.M., et al., 1991, A&ASS, 87, 361
Treffers R., Cohen M., 1974, ApJ 188, 545
Volk K.M., Kwok S., 1989, ApJ 342, 345
Waelkens C., Van Winckel H., Bogaert E., Trams N.R., 1991, A&A 251, 495
Waters L.B.F.M., Waelkens C., Trams N.R., 1992, A&A 262, L37
Weast R.C., 1992, CRC Handbook of Chemistry and Physics, 73rd ed., Chemical Rubber Co., Boca Raton
Webster A., 1993, MNRAS 264, 121
Webster A., 1995, MNRAS 277, 1555
Willner S.P., Jones B., Puetter R.C., Russell R.W., Soifer B.T., 1979, ApJ 234, 496